Visible and Near-Infrared Luminescence of Lanthanide-Containing Dimetallic Triple-Stranded Helicates: Energy Transfer Mechanisms in the Sm^{III} and Yb^{III} Molecular Edifices

Fabiana R. Gonçalves e Silva,[†] Oscar L. Malta,[‡] Christine Reinhard,[§] Hans-Ulrich Güdel,[§] Claude Piguet,[||] Jacques E. Moser,[⊥] and Jean-Claude G. Bünzli*,[†]

Swiss Federal Institute of Technology Lausanne, Institute of Molecular and Biological Chemistry, BCH, CH-1015 Lausanne, Switzerland, Departamento de Química Fundamental-UFPE, 50740-540 Recife, PE-Brazil, Department of Chemistry & Biochemistry, University of Bern, CH-3000 Bern 9, Switzerland, Department of Inorganic Chemistry, University of Geneva, CH-1211 Geneva-4, Switzerland, and Swiss Federal Institute of Technology Lausanne, Institute of Molecular and Biological Chemistry, Laboratory for Photonics & Interfaces, CH-1015 Lausanne, Switzerland

Received: July 26, 2001; In Final Form: November 20, 2001

The photophysical properties of the triple-stranded dimetallic helicates $[Ln_2(L^C-2H)_3]\cdot H_2O$ (Ln = Nd, Sm, Dy, Yb) are determined in water and D_2O solutions, and energy transfer processes are modeled for Sm^{III}. The luminescence of Nd^{III}, Sm^{III}, and Yb^{III} is sensitized by $(L^C-2H)^{2-}$, but the energy transfer from the ligand to the Ln^{III} ions is not complete, resulting in residual ligand emission. The luminescence of the Nd^{III} helicate is very weak due to nonradiative de-excitation processes. On the other hand, the Yb^{III} and Sm^{III} helicates exhibit fair quantum yields, 1.8% and 1.1% in deuterated water, respectively. The energy transfer rates between $(L^C-2H)^{2-}$ and Sm^{III} levels are calculated by direct and exchange Coulomb interaction models. This theoretical modeling coupled to numerical solutions of the rate equations leads to an estimate of the emission quantum yields in H_2O and D_2O, which compares favorably with experimental data. The main component of the ligand-to-metal energy transfer (97.5%) goes through a $^3\pi\pi^* \rightarrow {}^5G_{5/2}{}^{(1)}$ path, and the operative mechanism is of the exchange type. For the Yb^{III} helicate, minor effects of oxygen on the sensitization of Yb^{III} and nanosecond time-resolved spectroscopy point to the energy transfer mechanism being consistent with a recently proposed pathway involving fast electron transfer and Yb^{II}. No up-conversion process could be identified. Ligand-field splitting of the $^2F_{5/2}$ ($3E_{1/2} + E_{3/2}$) and $^2F_{7/2}$ ($2E_{1/2} + E_{3/2}$) levels of Yb^{III} is consistent with D_3 symmetry.

I. Introduction

Luminescent lanthanide-containing compounds present unique spectroscopic properties, such as long luminescent lifetimes and line-like emission of the metal ions. These features are presently used in the design of structural[1] and analytical[2] luminescent probes, labels for proteins and nucleic acids,[3] and of light-emitting sensors for hetero-[4] and homogeneous[5] fluoroimmunoassays. The development of Ln-containing responsive systems for biomedical analyses has long focused on Eu^{III} and Tb^{III} probes, as is the work aimed at engineering organic electroluminescent devices for light emitting diodes.[6] However, the need for multiple fluoroimmunoassays is now prompting the use of the luminescence of other Ln^{III} ions, for instance, Sm^{III} and Dy^{III},[7] while probing chiro-optical effects is leading to pioneer work with Ln^{III} ions emitting in the NIR, e.g., Yb^{III}.[8,9] The latter interest is further amplified by the development of organic lanthanide complexes for polymer-based optical amplifiers operating at 1.3 and 1.5 μm.[10]

We have recently synthesized a series of lanthanide dimetallic helicates $[Ln_2(L^C-2H)_3]\cdot nH_2O$ obtained by self-assembly process in water from ligand L^C and lanthanide salts, where L^C= bis{1-ethyl-2-[(6′-carboxy)pyridin-2′-yl]benzimidazol-5-yl}-methane (see Chart 1).[11] These molecular edifices represent a new class of highly stable carboxylates soluble in water, which is a mandatory characteristic for bioanalytical applications. In these triple-stranded helicates, the metal ion is well protected from solvent interaction and despite its lack of an efficient chromophoric substituent, $(L^C-2H)^{2-}$ sensitizes the Eu^{III} luminescence reasonably well.[11]

CHART 1

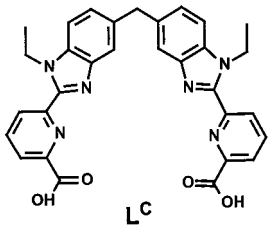

L^C

Since these helicates are stable and water-insensitive, we now examine the ability of $(L^C-2H)^{2-}$ to sensitize other Ln^{III} ions (Ln = Nd, Sm, Dy, and Yb) in aqueous solutions and in the pH range 7−12. The design of lanthanide-containing luminescent probes is not an easy task in view of the numerous energy transfer processes involved and of the many constraints on both the chemical and photophysical properties of the receptor.[12] Therefore, efficient modeling of these processes would bring a

* Corresponding author.
[†] Swiss Federal Institute of Technology Lausanne, BCH.
[‡] Departamento de Química Fundamental-UFPE.
[§] University of Bern.
[||] University of Geneva.
[⊥] Swiss Federal Institute of Technology Lausanne, Laboratory for Photonics & Interfaces.

10.1021/jp012884u CCC: $22.00
Published on Web 02/06/2002

better understanding of the crucial features needed and facilitate the choice of a convenient synthetic strategy. Such modeling has been proposed for Eu^{III} complexes,[13] and we have recently used this procedure to understand the luminescence quenching in a triple helical monometallic Eu^{III} complex with a ligand derived from bis(benzimidazole)pyridine (L).[14] We now extend this modus operandi to Sm^{III} and present, for the first time, calculations of energy transfer rates and emission quantum yields for this ion. The mechanism of Yb^{III} sensitization is also discussed on the basis of time-resolved spectroscopy.

II. Experimental Part and Methods

Syntheses. Ligand L^C was synthesized as previously described.[11] Solutions of the helicates were prepared as follows. A solution of L^C (6 mg, 0.010 mmol) in 4 mL of freshly bidistilled water or D_2O (99.99%, from ARMAR) was stirred at 295 K for 30 min; NaOH (from Merck) or NaOD (40% in D_2O, Fluka) was added dropwise, and the mixture was stirred at 295 K for 30 min. A solution of 0.007 mmol of $Ln(ClO_4)\cdot nH_2O$ (Ln = Sm, Yb, Dy, and Nd; n = 8.8, 6.34, 7, and 4.98, respectively) in 2 mL of water or D_2O was added dropwise, and the mixture was stirred for 2 h at 295 K. The solvents used to prepare these solutions were thoroughly degassed. The perchlorate salts $Ln(ClO_4)_3\cdot nH_2O$ were prepared from corresponding oxides (Rhône-Poulenc, 99.99%) in the usual way.[15] (Caution! Perchlorate salts combined with organic ligands are potentially explosive and should be handled in small quantities and with adequate precautions.[16]) The pH and pD of the solutions were adjusted with NaOH and NaOD, respectively, and were measured with a Metrohm 6.3013.210 glass electrode. The final pH was corrected for a deuterium isotope effect by using the equation pD = pH + 0.4.[17]

Physicochemical Measurements. UV/vis spectra were recorded at 22 °C on a Perkin-Elmer Lambda 900 spectrometer with the help of quartz cells of 1 and 0.1 cm path length. Excitation and emission spectra of the ligand and of its Sm^{III} complex were recorded on a Perkin-Elmer LS-50B spectrometer equipped for both room- and low-temperature measurements. The luminescence spectra of the Nd^{III} and Yb^{III} helicates were recorded with a Fluorolog-3 (TRIAXSERIES 320) spectrometer from Spex Industries. Luminescence and excitation spectra are corrected for the instrumental function. Lifetimes are averages of at least five independent determinations.

Continuous-wave luminescence and excitation measurements for the Yb^{III} helicate were performed by using a Ti:sapphire laser (Spectra Physics 3900S), pumped by an argon-ion laser (Spectra Physics 2060-10 SA) in all-lines mode. Wavelength control was achieved by an inchworm-driven (Burleigh PZ-501) birefringent filter, and the wavelength was monitored with a Burleigh WA2100 wavemeter. The sample luminescence was dispersed by a 0.85 m double monochromator (Spex 1402) using 500 nm blazed 1200 grooves/mm gratings and detected by a cooled photomultiplier (Hamamatsu 3310-01) and a photon-counting system (Stanford Research SR400). All the spectra were corrected for the sensitivity of the monochromator and detection system and for the refractive index of air (vacuum correction). They are represented as number of photons per second versus wavenumbers. The excitation spectra were corrected for the wavelength dependence of the output power of the Ti:sapphire laser.

The Yb^{III} lifetimes were measured both on the high-resolution instrument described earlier[11] and on a pulsed instrument. Pulsed laser excitation was applied to a sample solution, contained in a 1 cm quartz cell, using a frequency-tripled Q-switched Nd:YAG laser (Continuum Powerlite 7030, 30 Hz repetition rate, wavelength 355 nm, pulse width at half-height 7 ns). The pulse energy was typically restricted to less than 5 mJ to prevent rapid degradation of the sample. The emission from the solution was collected at right angle to the excitation beam by a 2″ plano-convex lens, passed through various optical elements, a $^1/_8$ m grating monochromator (Oriel model 77250) and was finally detected by a fast red-sensitive photomultiplier tube (Hamamatsu R928), only three dynodes of which were employed. Light scattered by the sample and the cell walls was blocked before the monochromator by a 400 nm cutoff filter. A 1 GHz band-pass digital signal analyzer (Tektronix DSA 602A) was employed to record the time course of the laser-induced emission. Satisfactory signal-to-noise ratios were typically obtained by averaging over several hundreds laser shots.

The quantum yields were calculated using the following equation:

$$Q_x/Q_r=[A_r(\lambda_r)/A_x(\lambda_x)][I(\lambda_r)/I(\lambda_x)][n_x^2/n_r^2][D_x/D_r]$$

in which subscript r stands for the reference and x for the samples; A is the absorbance at the excitation wavelength, I is the intensity of the excitation light at the same wavelength, n is the refractive index (n = 1.328, in D_2O, and n = 1.333, in H_2O), and D is the measured integrated luminescence intensity. Emission band areas were corrected, when needed, for the Raman and Rayleigh diffusion bands, by subtracting the spectrum of the solvent alone. Concentrations and excitation wavelengths of the reference and sample were chosen to generate an absorbance < 0.05, for which a linear relationship between the intensity of the emitted light and the concentration of the absorbing species is found.[18] Degassed solvents were used to avoid a possible quenching of the ligand triplet state by oxygen. The standards used to determine the quantum yield of the Sm^{III} helicate were quinine sulfate in 0.5 M H_2SO_4 (n = 1.338, Q_{abs}= 0.546[19]), cresyl violet 1.4×10^{-5} M in MeOH (n = 1.329, Q_{abs}= 0.54[20]), and $[Ru(bipy)_3]^{2+}$ 6×10^{-5} M in water (n = 1.333, Q_{abs}= 0.042[21]), where bipy stands for 2,2′-bipyridine. These standards possess an absorbance in the UV region similar to that of the Sm^{III} helicate, and the last two ones exhibit emission in the same wavelength range than Sm^{III}. Ligand-centered luminescence was measured relative to quinine sulfate in 0.5 M H_2SO_4. The $[Yb(TTA)_3]$ complex, TTA = thenoyltrifluoroacetonate, was used as reference to determine the quantum yield of the metal-centered luminescence in $[Yb_2(L^C-2H)_3]$. The $[Yb(TTA)_3]$ complex was synthesized according to the published method.[22] The emission quantum yield of this complex in toluene solution (n = 1.4964) was taken as Q_{abs}= 0.35%.[23]

Theoretical Models Used.[13,24] As previously shown, the various contributions to the ligand-to-rare earth ion energy transfer rates W_{ET} may be described by the following expressions 1−3:[25]

$$W_{ET}^{mp}=\frac{2\pi}{\hbar}\frac{e^2S_L}{(2J+1)G}F\sum_\lambda \gamma_\lambda \langle \alpha' J'||U^{(\lambda)}||\alpha J\rangle^2 \qquad (1a)$$

describes the contribution of the dipole-2^λ pole mechanism (λ = 2, 4, and 6), with

$$\gamma_\lambda=(\lambda+1)\frac{\langle r^\lambda\rangle^2}{(R_L^{(\lambda+2)})^2}\langle 3||C^{(\lambda)}||3\rangle^2(1-\sigma_\lambda)^2 \qquad (1b)$$

TABLE 1: Values of the Matrix Elements Used in the Analysis of the Energy Transfer Process in the Sm^{III} Helicate

	$\lambda = 2$	$\lambda = 4$	$\lambda = 6$	
$\langle {}^6H_{5/2}\|\|U^\lambda\|\|{}^4H_{9/2}\rangle^2$ [a]	0.0001	0.0002	0.0006	$\langle {}^6H_{5/2}\|\|S\|\|{}^4G^{(1)}_{5/2}\rangle = 0.78$ [b]
$\langle {}^6H_{5/2}\|\|U^\lambda\|\|{}^4H_{13/2}\rangle^2$ [a]	0.0	0.0	0.0002	$\langle {}^6H_{5/2}\|\|S\|\|{}^4G^{(2)}_{5/2}\rangle = 0.12$ [b]
$\langle {}^6H_{5/2}\|\|U^\lambda\|\|{}^4G_{9/2}\rangle^2$ [a]	0.0001	0.0009	0.0013	$\langle {}^6H_{5/2}\|\|L + 2S\|\|{}^4G^{(1)}_{5/2}\rangle = 1.05$ [b]
$\langle {}^6H_{5/2}\|\|U^\lambda\|\|{}^4I_{9/2}\rangle^2$ [a]	0.0022	0.0005	0.0014	
$\langle r^\lambda \rangle$	2.73×10^{-17} cm^2	1.77×10^{-33} cm^4	2.31×10^{-49} cm^6	

[a] Matrix elements of U^λ for Sm^{III}(aq) obtained from ref 31. [b] Obtained by using the wave functions of Sm^{III} in SmOCl.

where $\langle r^\lambda \rangle$ is the radial expectation value of r^λ for 4f electrons, C^λ is a Racah tensor operator, and

$$F = \frac{1}{\hbar \Delta A_L} \sqrt{\frac{\ln 2}{\pi}} \exp\left[-\left(\frac{\Delta E}{\hbar \Delta A_L} \right)^2 \ln 2 \right] \qquad (1c)$$

where ΔE is the energy difference between the ligand donor level and the lanthanide ion acceptor level and ΔA_L is the bandwidth at half-height of the ligand state

$$W_{ET}^{dp} = \frac{2\pi}{\hbar} \frac{e^2 S_L}{(2J+1) G R_L^6} F \sum_\lambda \Omega_\lambda^{e.d.} \langle \alpha' J' || U^{(\lambda)} || \alpha J \rangle^2 \qquad (2)$$

corresponds to the dipole−dipole mechanism (λ = 2, 4, and 6), and

$$W_{ET}^{ex} = \frac{8\pi}{3\hbar} \frac{e^2 (1-\sigma_0)^2}{(2J+1) R_L^4} F \langle \alpha' J' || S || \alpha J \rangle^2 \times \sum_m |\langle \phi | \sum_k \mu_Z(k) s_m(k) | \phi' \rangle|^2 \qquad (3)$$

represents the exchange mechanism. In the above equations, J is the total angular momentum quantum number of the rare-earth ion and α specifies a 4f spectroscopic term. G is the degeneracy of the ligand initial state, and S_L is the electric dipole strength associated with the transition $\phi \rightarrow \phi'$ in the ligand. The quantities $\langle || \, || \rangle$ are reduced matrix elements of the unit tensor operators $U^{(\lambda)}$,[26] and R_L is the distance from the rare-earth ion nucleus to the region of the ligand molecule in which the ligand donor (or acceptor) state is localized.[27] In eq 3, S is the total spin operator of the rare-earth ion, μ_Z is the z component of the electric dipole operator, s_m ($m = 0, \pm 1$) is a spherical component of the spin operator for the ligand electrons, and σ_0 is a distance-dependent screening factor.[28]

The matrix elements $\langle \phi | \sum_k \mu_Z(k) s_m(k) | \phi' \rangle$ were calculated from the molecular orbital wave functions given by the Sparkle model,[29,30] which optimizes the coordination geometry and electronic structure of the organic part of the complex. The quantities γ_λ and F were previously described.[29] The selection rules that can be derived from the above equations are the following: $J + J' \geq \lambda \geq |J - J'|$ for the mechanisms expressed by eqs 1 and 2, and $\Delta J = 0, \pm 1$ for the exchange mechanism; in both cases, transitions with $J' = J = 0$ are excluded. The selection rules for the ligand levels involved can be derived from the electric dipole strength S_L and the matrix element of the coupled operators μ_Z and s_m in eq 3.

The normalized populations of the electronic levels, η_i, are described by

$$\frac{d\eta_i}{dt} = -\sum_{\substack{j=1 \\ j \neq i}}^{N} k_{ij} \eta_i + \sum_{\substack{j=1 \\ j \neq i}}^{N} k_{ji} \eta_j \qquad (4)$$

where the indices i and j indicate the energy levels involved in the energy transfer process. The k_{ij} or k_{ji} symbols correspond to the decay rate constants between i and j or j and i levels, respectively, and N is the total number of levels involved. In the steady-state regime, all $d\eta_i/dt$ are equal to zero, and the set of algebraic equations can be solved analytically in terms of the transition and transfer rates. In the present case, the rate equations were solved numerically by using fourth-order Runge−Kutta method with an adaptive integration step.[27] This set of coupled differential equations belongs to the initial value category, where the populations (η_i) at $t = 0$ are set equal to 1 for the ground state population and to zero for the other states. The total time of propagation was around 0.01 s, and the initial step size was equal to the inverse of the largest transfer rate constant (approximately 10^{-9} s). The numerical solutions of the rate equations yield the time dependence of the energy level populations, which reach the steady-state regime after 10^{-6} to 10^{-5} s.

Modeling Energy Transfer Processes in the Sm^{III} Helicate. We have applied the above theory for the first time to analyze the energy transfer processes in a Sm^{III} compound. The required parameters are listed in Table 1.

The criteria used to determine which of the Sm^{III} excited levels could be potentially involved in the ligand-to-metal transfer processes were the following:

1. The energy differences $\Delta E({}^1\pi\pi^* - {}^{(2S+1)}\Gamma_J)$ or $\Delta E({}^3\pi\pi^* - {}^{(2S+1)}\Gamma_J)$ have been set to $\Delta E \leq \Delta A_L/2$, to allow for a sufficient spectral overlap integral (Förster's theory); $\Delta A_L/2$ is around 2200 and 2100 cm^{-1} for the emission bands corresponding to ${}^1\pi\pi^*$ and ${}^3\pi\pi^*$ states, respectively. According to this criterion, Sm^{III} levels[31] with energy in the ranges 28100−32500 and 16500−20700 cm^{-1} only show appropriate resonance conditions and were taken into consideration.
2. In the case of Sm^{III}, the selection rules derived for multipolar ($\Delta J = 2, 4, 6$) and exchange ($\Delta J = 0, \pm 1$) mechanisms further restrict the number of levels to 6 and 8, respectively.
3. For multipolar mechanisms, only four levels have significant matrix elements $U^{(\lambda)}$: ${}^4I_{9/2}$, ${}^4H_{9/2}$, ${}^4H_{13/2}$, and ${}^4G_{9/2}$. For the exchange mechanism, only two levels have a reduced matrix element $\langle \alpha' J' || S || \alpha J \rangle \neq 0$: ${}^4G_{5/2}{}^{(1)}$ (ca. 17900 cm^{-1}) and ${}^4G_{5/2}{}^{(2)}$ (ca. 30230 cm^{-1}).

III. Photophysical Properties

Ligand-Centered Properties. Ligand L^C is stable in H_2O and D_2O solutions and displays three main absorption bands around 48000, 40000, and 32460 cm^{-1}, which are almost pH insensitive in the range 7−12. The emission of the singlet state occurs around 25000 cm^{-1} upon excitation at 38500 cm^{-1} and the lifetime (τ_S) of this emission is 8 ns (Table 2). The quantum yield of uncoordinated L^C, measured at pH or pD 7.5 and under excitation at $\tilde{\nu}_{ex} = 29400$ cm^{-1} (Table 2) is 2.4 times larger in D_2O (12%) compared to H_2O (5%), supporting the explanation put forward previously that strong water interaction with the

TABLE 2: Absolute Quantum Yields ($Q_{Abs} \pm 20\%$) of the Metal-Centered Luminescence in the Sm^{III} and Yb^{III} Helicates, of the Ligand-Centered Luminescence for Free and Complexed $(L^C-2H)^{2-}$ in the Dy^{III}, Sm^{III}, and Yb^{III} Helicates, and Lifetimes (τ) of Sm^{III}, Yb^{III}, and L^C, in Solution at 295 K

compound[a]	solvent	c/M	$\tilde{\nu}_{exc}$/cm^{-1}	Q^{Ln}_{abs}/%	Q^{L}_{abs}/%	$\tau/\mu s$ [b]
$[Sm_2(L^c-2H)_3]$	D_2O	3.1×10^{-6}	27550	1.1	0.11	180 ± 1
	H_2O	4.0×10^{-6}	27550	0.14	0.03	42.0 ± 0.4
$[Yb_2(L^c-2H)_3]$	D_2O	5.1×10^{-6}	32250	1.8	0.20	40 ± 2
$[Dy_2(L^c-2H)_3]$	D_2O	2.0×10^{-6}	26700	--	0.18	--
	H_2O	1.1×10^{-6}	27000	--	0.08	--
L^c	D_2O	8.8×10^{-7}	29410	--	12	0.008 ± 0.0006
	H_2O	8.0×10^{-7}	29410	--	5.0[c]	--

[a] At pH or pD 7.5. [b] Obtained monitoring the $Sm(^4G_{5/2} \rightarrow {}^6H_{7/2})$ transition, the $^1\pi\pi^*$ ligand emission, and the $Yb(^2F_{5/2} \rightarrow {}^2F_{7/2})$ transition. [c] As compared to 5.5% reported in ref 11.

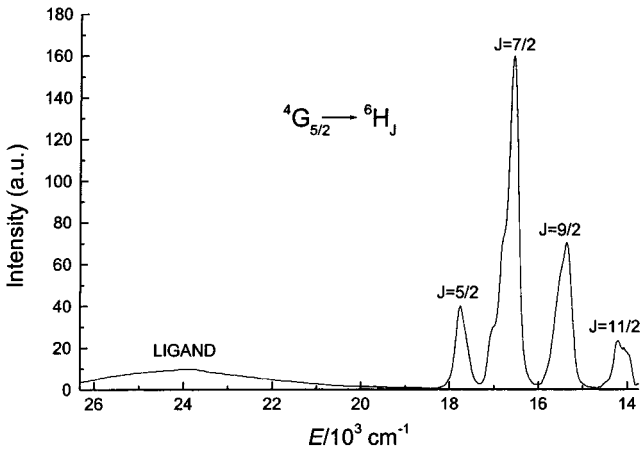

Figure 1. Emission spectrum of the $[Sm_2(L^C-2H)_3]$ in D_2O upon excitation at 27250 cm^{-1}, at 295 K and pD = 7.5.

carboxylic groups contributes to luminescence quenching in H_2O.[11]

Upon formation of the $[Ln_2(L^C-2H)_3]$ helicates, the lower-energy $\pi \rightarrow \pi^*$ transition of the $[L^C-2H]^{2-}$ moieties undergoes a red shift of 2400 cm^{-1} with the appearance of a shoulder on its high-energy side, while the absorption band of the higher energy transition occurs around 50000 cm^{-1}. Weak ligand-centered luminescence is seen for all the helicates, centered around 24000 cm^{-1} and with a quantum yield about 2 orders of magnitude smaller compared to that of the free ligand. For Nd^{III}, Sm^{III}, and Yb^{III}, metal-centered luminescence occurs as well; it is extremely weak for Nd^{III} but is not observed at all for Dy^{III}. Given that the triplet state emission from the ligand at 77 K is also much weaker in the Dy^{III} helicate than in the free ligand while no metal-centered luminescence is seen, we conclude that energy transfer does occur from the ligand to the Dy^{III} ion, but that the energy is then dissipated through nonradiative processes. A similar explanation is valid for the Nd^{III} helicate. These two compounds were not further investigated in view of their poor luminescent properties.

Metal-Centered Photophysical Properties. The emission spectrum of the Sm^{III} helicate is reported in Figure 1. It displays four main bands at 17762, 16584, 15361, and 14205 cm^{-1}, corresponding to the $^4G_{5/2} \rightarrow {}^6H_{5/2}$, $^4G_{5/2} \rightarrow {}^6H_{7/2}$, $^4G_{5/2} \rightarrow {}^6H_{9/2}$, and $^4G_{5/2} \rightarrow {}^6H_{11/2}$ transitions, respectively, in addition to the weak fluorescence band from the ligand at 23810 cm^{-1}. The ratio of the emission intensities as measured by the band areas, $I(^4G_{5/2} \rightarrow {}^6H_J)/I(^1\pi\pi^*)$ amounts to 2.3 in D_2O. The quantum yield of the $^1\pi\pi^*$ emission in $[Sm_2(L^C-2H)_3]$ is 110 (D_2O) and 170 (H_2O) times smaller compared to uncoordinated $(L^C-2H)^{2-}$. On the other hand, we have determined the quantum yield of the metal-centered luminescence at pH 7.5, under excitation at 27550 cm^{-1}. Three different standards were used, leading to very similar values with averages of 1.1% in D_2O and 0.14% in H_2O (6 determinations). In summary, and roughly speaking, complexation of the Sm^{III} ion results in more than 99% of the energy of the excited ligand state being transferred onto the metal ion; on the other hand, only a very small part is emitted in a radiative way by Sm^{III}.

It is noteworthy that the quantum yields determined can be considered as being relatively large for a Sm^{III}-containing compound: the energy gap between the lowest sublevel of $^5G_{5/2}{}^{(1)}$ and the highest sublevel of the ^6F multiplet, $^6F_{11/2}$, is known to be around 7400 cm^{-1}, which favors nonradiative deexcitation processes, especially in compounds with organic ligands possessing several vibrations of relatively high energy. As a comparison, a quantum yield of 0.20% in water has been reported for the Sm^{III} complex with a pyrazole-containing ligand, *N,N,N′,N′*-{2,6-bis[3-(aminomethyl)pyrazol-1-yl]pyrazine}tetrakis-(acetic acid), L^1,[32] which displays good chromophoric and energy transfer properties, while a quantum yield of 2% has been reported for an especially well protected micellar system suitable for fluoroimmunoassays and containing 1,1,1-trifluoro-4-(2-naphthyl)-butane-2,4-dione, trioctylphosphine oxide and Triton X-100.[4]

The lifetime of the $^4G_{5/2}^{(1)}$ level increases from 42 to 180 μs in going from H_2O to D_2O. Using Kimura's equation,[33] we calculate that essentially no water is bound into the first coordination sphere, in line with previous observations for the Eu^{III} and Tb^{III} helicates.[11] Therefore, the large effect of H_2O on the radiative rate constant is due to second-sphere interactions. The lifetime of 180 μs in D_2O is long, compared with $^4G_{5/2}^{(1)}$ lifetimes reported previously: 79-96 μs in several systems used for fluoroimmunoassays and containing a β-diketonate, Triton X-100 and Y^{III} as co-luminescence enhancement ion,[34] 86 μs for Sm^{III} chelated by 2-naphthoyltrifluoroacetone in benzene[35], and 30 μs for the complex with ligand L^1.[32]

A relatively intense metal-centered NIR emission is observed for the Yb^{III} helicate in D_2O upon excitation at 32258 cm^{-1}, while it is extremely weak in H_2O, which prevented us to measure the corresponding lifetime. The spectrum is depicted in Figure 2. It displays a band centered at ca. 10000 cm^{-1} with four main components at 10493 (2′−0), 10224 (0′−0), 10091 (0′−2), and 9852 (0′−3) cm^{-1}, assigned to the $^2F_{5/2} \rightarrow {}^2F_{7/2}$ transitions. They arise from the M_J splitting of the emitting and/or fundamental state, as a consequence of ligand field effects. The line at 10224 cm^{-1} corresponds to the lowest component of $^2F_{5/2}$, since at this wavelength the excitation and emission lines overlap. Excitation spectrum in the infrared region of the Yb^{III} helicate, recorded by monitoring the emission from Yb^{III} at 10200 cm^{-1}, presents three very weak bands centered at 10500, 10800, and 11110 cm^{-1} (right side of Figure 2, see scale). Only the first one is of electronic nature, the latter two being of vibronic origin. The total ligand-field splitting amounts

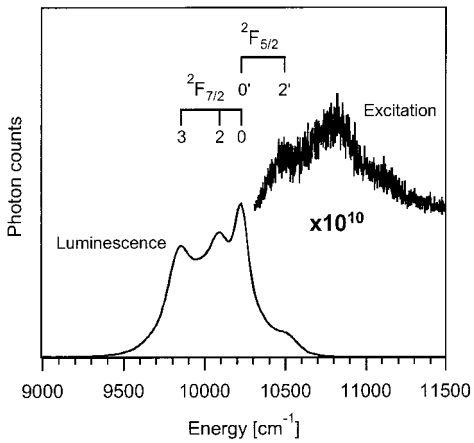

Figure 2. Spectra of $[Yb_2(L^C-2H)_3]$ in D_2O. Left: emission spectrum at 295 K and pD = 7.5 upon excitation at 32258 cm^{-1}. Right: excitation spectrum obtained by analyzing the infrared emission at 10200 cm^{-1}, at 15 K and pD = 7.5. The level numbering refers to the emission spectrum.

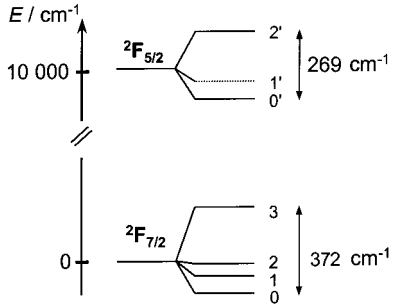

Figure 3. Ligand-field sublevels of Yb^{III} in $[Yb_2(L^C-2H)_3]$, as determined from emission and excitation spectra at 295 and 15 K, respectively. Level 1′($^2F_{5/2}$) has not been formally identified.

to 269 and 372 cm^{-1} for the $^2F_{5/2}$ and $^2F_{7/2}$ levels, respectively (Figure 3). Analyzing these splittings in terms of group theory allowed us to assess the site symmetry of the Yb^{III} ions, which is consistent with D_3. Determination of the irreducible representations of the angular momentum operator J in this symmetry leads to four sublevels ($3E_{1/2} + E_{3/2}$) for $^2F_{7/2}$ and three sublevels ($2E_{1/2} + E_{3/2}$) for $^2F_{5/2}$. This is in agreement with the number of experimentally determined sublevels, with paramagnetic NMR measurements indicating that the helicates retain time-averaged D_3 symmetry along the entire Ln^{III} series,[36] and with the X-ray crystal structure of the Yb^{III} helicate.[11] Up-conversion processes have been evidenced in Yb dimers in nonmolecular ionic lattices.[37] To investigate whether such a process takes place in the Yb^{III} helicate, we have recorded its emission spectrum upon direct metal excitation in the infrared region, at $\tilde{\nu}_{exc}$ = 10753 cm^{-1}, but no visible emission was observed. A definitive conclusion cannot, however, be drawn from this experiment: in ionic systems, the photon ratio between visible and NIR emission is around 10^{-6},[37] and if it does exist, we expect a less efficient up-conversion process in the dimetallic helicate in view of the large $Yb^{III}-Yb^{III}$ separation (9.1−9.3 Å[11]) so that an extremely faint signal would be expected. On the other hand, direct metal excitation leads to a very weak Yb^{III}-centered emission, compared with ligand excitation, in line with the very weak excitation spectrum shown on Figure 2. This points to an appreciable sensitization of the Yb^{III} by the ligand, as shown by the following data.

The lifetime of the Yb($^2F_{5/2}$) state is long in D_2O, 40 μs (Table 2) compared to solution data reported previously, e.g., 18.6 μs in DMSO−d_6 for a *m*-terphenyl-based complex bearing a triphenylene chromophore[38] and 6.2 μs in D_2O for a complex with a chiral macrocyclic tetra-amide.[39] As a result, the quantum yield of the metal-centered luminescence amounts to 1.8% (D_2O) upon ligand excitation which, again is fairly large compared with the values reported in the literature for other Yb^{III} complexes, e.g., 0.45% for the complex with fluorexon in D_2O[40] or 0.5% for a terphenyl-based complex in DMSO.[41]

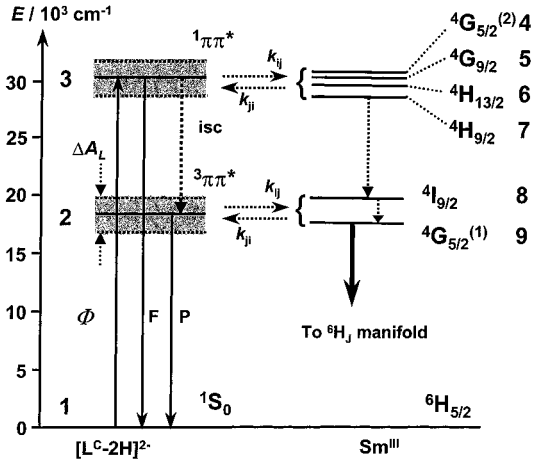

Figure 4. Schematic and partial diagram of the main energy transfer processes in $[Sm_2(L^C-2H)_3]$. The solid and dashed arrows represent radiative and nonradiative processes, respectively. Key: F, fluorescence; P, Phosphorescence; isc, intersystem crossing; Φ, photon flux; ΔA_L, see eq 1b.

The metal-centered emission quantum yields for the Sm^{III} and Yb^{III} helicates are large, compared to literature data, despite their absolute low values. Usually the nonradiative de-excitation of the metal-ion emitter level is related to the energy gap between the lowest luminescent excite state and the highest sublevel of the ground multiplet. These gaps amount to ∼7400 cm^{-1} for the $^4G_{5/2} \rightarrow {}^6F_{11/2}$ transition of Sm^{III} and to ∼10200 cm^{-1} for the $^2F_{5/2} \rightarrow {}^2F_{7/2}$ transition of Yb^{III}.[42] Therefore, overtones and/or combinations of high-energy vibrational modes, such as C−H and C═O oscillators, are in principle able to match these gaps, resulting in efficient quenching of the luminescent states. Such quenching mechanisms appear however to be not very efficient in the studied helicates given that the lifetimes, which are among the largest reported for Sm^{III} [33−35] and Yb^{III} compounds, are quite longer in D_2O compared to H_2O. This can be traced back to the rigidity of the coordination environment in these molecular dimetallic edifices.

IV. Modeling of the Energy Transfer Processes

We have attempted to rationalize the quantitative data described above for Sm^{III} and Yb^{III} by an adequate modeling. The diagram sketched in Figure 4 shows the energy transfer processes taken into consideration for the sensitization of the Sm^{III} compound. This model is based on the observed photophysical properties of this helicate and allows ligand-to-metal energy transfers to occur through either the singlet or triplet state. The initial excitation takes place through UV absorption by the lower energy singlet state of the $(L^C-2H)^{2-}$ moieties. The second singlet state, around 50 000 cm^{-1} (Table 3), was not taken into consideration, since experimental quantum yield were determined upon excitation around 28000 cm^{-1}. The singlet state is then deactivated by three main paths: (i) decay to the ground state (radiative and nonradiative), (ii) intersystem crossing to the triplet state, followed either by transfer onto the metal ion or by decay to the ground state, and (iii) energy transfer to high energy level(s) of the lanthanide ion. The second

TABLE 3: Experimental Transition Energies (cm^{-1}) from and to the Singlet and Triplet States of $[Ln_2(L^c-2H)_3]$

triplet state[a]	singlet state[b]	
Ln = Gd	Ln = Sm	Ln = Yb
16560	28490 sh	28460 sh
17950	30300	30380
19340	34600 sh	34550 sh
20660	40065 sh	40000 sh
	50000	50250

[a] From phosphorescence spectra at 10 K for Gd helicate, obtained from ref 11. [b] From absorption spectra in H_2O at 293 K; sh = shoulder.

process is important for lanthanide containing compounds because intersystem crossing rates (isc) are enhanced by paramagnetic and heavy atom effects.[43] This is exemplified by the quantum yield of the ligand-centered fluorescence of the Gd^{III} helicate in H_2O which amounts to only 0.93%,[11] down from 5% for the free ligand. A similar, but much more pronounced trend is observed for the Sm^{III} helicate that presents a very small quantum yield in D_2O, 0.03%, compared to 12% for the free ligand. These data point to the intersystem crossing in the ligand increasing upon complexation with a concomitant energy transfer onto the metal ion and a large decrease in the emission from the singlet state.

The Sm^{III} ion possesses a wealth of electronic levels, which have been identified and labeled by Carnall et al.[31] We have used several criteria to select the levels most amenable to energy transfer, in particular resonance conditions and selection rules (see Experimental Section), which limited the number of potentially interesting levels to six: (i) an exchange mechanism is operative for the two $^4G_{5/2}$ levels (30230 and 17900 cm^{-1}), and multipolar mechanisms are effective for the $^4I_{9/2}$, $^4H_{9/2}$,$^4H_{13/2}$, and $^4G_{9/2}$ levels. To apply the selection rules, we have considered solely the ground state $^6H_{5/2}$; at room temperature, population of the $^6H_{7/2}$ level is around 0.06% only, and we think that the benefit introduced by taking the latter level into consideration would have been largely outbalanced by the severe complications brought in the model.

The parameters used in the calculation of the energy transfer rate constants and quantum yield were the following: A_T (spontaneous emission coefficient) = 880 s^{-1} and $1/\tau = 23998$ s^{-1} in H_2O, and $A_T = 894$ s^{-1} and $1/\tau = 5531$ s^{-1} in D_2O. The $^4G_{5/2} \rightarrow {}^6H_{5/2}$ transition was taken as reference in the estimate of the spontaneous emission coefficient because the quantities $U^{(\lambda)}$ are very small for this transition. The R_L and $\langle\phi|\sum_k \mu_Z(k)\text{-}s_m(k)|\phi'\rangle$ values have been calculated previously for the following compounds: $[Eu(NO_3)_3L(MeOH)]$,[14] $Eu(TTA)_3{\cdot}2H_2O$ and $Eu(TTA)_3{\cdot}2DBSO$,[29] where L = 2,6-bis(1-methylbenzimidazol-2-yl)pyridine, TTA= thenoyltrifluoroacetonate and DBSO = dibenzyl sulfoxide. In these compounds, R_L ranges between 4.3 and 4.5 Å and $\langle\phi|\sum_k \mu_Z(k)s_m(k)|\phi'\rangle$ between 0.8×10^{-36} and 1.9×10^{-36} esu^2 cm^2. In view of their relative insensitivity to the nature of the complex, we have chosen the same values as those calculated by the Sparkle model for $[Eu(NO_3)_3L(MeOH)]$, 4.3 Å and 1.9×10^{-36} esu^2 cm^2, respectively.[14] The other parameters were set to $\Delta A_L(^3\pi\pi^*) = 4200$ cm^{-1}, from the phosphorescence spectra of the Gd^{III} helicate,[11] $\Delta A_L(^1\pi\pi^*) = 4400$ cm^{-1}, from the absorption band of the lower energy singlet centered at 30300 cm^{-1}, and $\sigma_0 = 0.99$, from the structural data reported for the Eu^{III} and Tb^{III} helicates.[11] The transfer rate constant $k_{13} = \phi = 10^4$ s^{-1} was assumed to be identical with those found for other coordination compounds,[7] while the rate constants for nonradiative decays from the excited Sm^{III} levels have been set to 10^6 s^{-1}.[44]

TABLE 4: Calculated Energy Transfer Rates (s^{-1}) for $[Sm_2(L^c-2H)_3]$

$E(L^C$ state)/ cm^{-1}		E(4f state) / cm^{-1}	transfer rate W_{ET}/s^{-1}	back-transfer rate W_{BT}/s^{-1}
$^3\pi\pi^*$ (18 620)	→	$^4G^{(1)}_{5/2}$ (17900)	8.4×10^9	2.72×10^8
$^3\pi\pi^*$ (18 620)	→	$^4I_{9/2}$ (20500)	4.67×10^6	601
$^1\pi\pi^*$ (30 300)	→	$^4H_{9/2}$ (29000)	6.0×10^5	1.23×10^3
$^1\pi\pi^*$ (30 300)	→	$^4H_{13/2}$ (29800)	1.37×10^5	1.27×10^4
$^1\pi\pi^*$ (30 300)	→	$^4G_{9/2}$ (30100)	1.52×10^6	5.87×10^5
$^1\pi\pi^*$ (30 300)	→	$^4G^{(2)}_{5/2}$ (30232)	1.75×10^8	1.27×10^8

TABLE 5: Calculated Quantum Yield (%) of $[Sm_2(L^c-2H)_3]$ at 300 K for Several Values of the Transition Rates[a]

k_{31} (s^{-1})	k_{21} (s^{-1})	k_{32} (s^{-1})	$Q(D_2O)$	$Q(H_2O)$
10^5	10^7	10^8	0.271	0.253
10^6	10^7	10^8	0.27	0.25
10^7	10^7	10^8	0.25	0.23
10^8	*10^7*	*10^8*	*0.14*	*0.12*
10^9	10^7	10^8	0.025	0.024
10^8	10^5	10^8	5.2	1.6
10^8	*10^6*	*10^8*	*1.2*	*0.79*
10^8	10^8	10^8	0.013	0.014
10^8	10^9	10^8	0.0014	0.0014
10^8	10^7	10^5	0.0070	0.0065
10^8	10^7	10^6	0.0093	0.0086
10^8	10^7	10^7	0.030	0.028
10^8	10^7	10^9	0.25	0.23
experimental data			1.1	0.14

[a] See Figure 4 for the numbering of the states and, therefore, the labeling of the rate constants. Italicized values reproduce best the experimental data.

The theoretical values for the forward and back-transfer rate constants calculated from eqs 1−3 are listed in Table 4. They vary widely for the different levels involved, between 10^5 and 10^9 s^{-1}, a range comparable to that found for the transfer rate constants in the 1:1 and 1:3 complexes of Eu^{III} with L.[45] The largest rate constants correspond to both $^4G_{5/2}$ levels and a first conclusion is that these levels are implicated in the main path(s) of the energy transfer process. The numerical solutions of the rate equations were used to calculate the populations of the levels (eq 4) which, in turn, were used to estimate the emission quantum yields.

We have performed a variable analysis to investigate the dependence of the quantum yield upon the rate constants k_{21}, k_{31}, and k_{32} (Table 5). A quite satisfactory match between the calculated (1.2%) and experimental (1.1%) quantum yields in D_2O solution was found by setting $k_{21} = 10^6$ s^{-1}, $k_{31} = 10^8$ s^{-1}, and $k_{32} = 10^8$ s^{-1}. For H_2O solution, $k_{21} = 10^7$ s^{-1}, $k_{31} = 10^8$ s^{-1}, and $k_{32} = 10^8$ s^{-1} gave a calculated quantum yield = 0.12%, as compared to 0.14% for the experimental one. It is noteworthy that, as expected, the only rate constant influenced by the solvent change is k_{21}, which becomes 10 times larger in H_2O compared to that in D_2O, while the intersystem crossing rate constant remains the same (10^8 s^{-1}) and is comparable to that found in the complexes with L (10^7−10^8 s^{-1})[45] and in metallotexaphyrins containing coordinated Nd^{III} and Y^{III} ions.[46] This means that second sphere interactions of water molecules with the carboxylic groups not only depopulate the emitter level of the Sm^{III} ion, but also the triplet state level, consistent with the quantum yields for the ligand-centered luminescence discussed above. The large k_{32} value is typical of a heavy-atom effect.[43]

The lifetime of the $^1\pi\pi^*$ emission in the helicate depends on the energy transfer rate constants to the Sm^{III} upper excited

levels, on k_{32}, and on the internal conversion rate constant k_{31}. The same lifetime in the uncoordinated ligand depends only on k_{31} and k_{32}, and the latter rate constant is smaller in the ligand than in the complex, as describe above. Therefore, the internal conversion rate constant k_{31} in the Sm^{III} helicate should be comparable to the inverse of the singlet emission lifetime ($1/\tau_S$) in the uncoordinated ligand, which is the case: $1/\tau_S = 1.2 \times 10^8$ s^{-1} compares well with the k_{31} value of 10^8 s^{-1} reproducing best the experimental quantum yields in both water and deuterated water.

Finally, we have evaluated the contributions of the various energy-transfer processes to the overall quantum yield by performing the theoretical calculations for each separate level. It turns out that $^3\pi\pi^* \rightarrow {}^4G_{5/2}{}^{(1)}$ accounts for ca. 97.5% of the total energy transfer while $^1\pi\pi^* \rightarrow {}^4G_{5/2}{}^{(2)}$ accounts for 1% and all the other processes for the remaining 1.5%. Therefore, the common, and simplified, thinking that ligand-to-metal energy transfers in lanthanide-containing compounds goes essentially through the triplet state is validated in our particular case. One difference is that the main operative mechanism is an exchange one and not a Förster-type mechanism, pointing to some orbital overlap between the ligand and 4f states.

The Yb^{III} helicate in D_2O presents a much stronger metal-centered emission in the infrared upon ligand excitation than upon direct excitation of the metal ion, clearly establishing the sensitizing role of the ligand. The oxygen effect on the sensitized luminescence intensity and time-resolved luminescence were investigated with the objective of determining which energy transfer mechanism is operative in this compound, since there is very little overlap between the ligand $^1\pi\pi^*$ and $^3\pi\pi^*$ states and the $^2F_{5/2}$ level. Oxygen may deactivate the triplet level, and if the main path of the ligand-to-metal energy transfer goes through the $^3\pi\pi^*$ level, this is reflected in a concomitant decrease in the lanthanide-centered emission. The emission spectra of the Yb^{III} helicate were therefore measured for both deaerated and nondegassed solutions and they did not show significant intensity change. The rate constant of oxygen quenching of the triplet state (k_{ox}) is equal to the product of the diffusion-controlled quenching rate constant by the oxygen concentration, $k_{ox} = k_{diff}[O_2]$. In D_2O, $[O_2] = 0.265$ mM[47] and k_{diff} is on the order of 10^{10} M^{-1} s^{-1};[38] therefore, $k_{ox} = 2.7 \times 10^6$ s^{-1}. Since oxygen has no effect on the metal-centered luminescence of the Yb^{III} helicate, W_{ET} must be significantly larger than k_{ox}. This is unexpected given that the energy transfer rate constant of the triplet state to the $^2F_{5/2}$ emitter level is usually considered to be 10^6 s^{-1},[38] in view of the extremely small spectral overlap between the emission spectrum from the triplet state and the absorption spectrum of the Yb^{III} ion.[38,41,41] One may therefore suspect that another mechanism is operative for the ligand-to-Yb^{III} energy transfer. In the cases of lanthanide chelates bearing an aromatic side-chain[48] and of complexes with proteins,[49] other authors have proposed that sensitization of Yb^{III} occurs via a long-range electron transfer process involving Yb^{II}. Such a mechanism has been confirmed for a variety of complexes.[49] More recently, ultrafast time-resolved spectroscopy has also authenticated this mechanism for the (bipy.bipy.bipy) cryptand.[9] We have investigated the Yb^{III} helicate under similar experimental conditions and found that the rise time of the metal-centered emission is extremely fast ($\tau_{rise} < 8$ ns). In summary, this information, combined with the absence of oxygen quenching and the fact that the intensity of the $^1\pi\pi^*$ emission decreases drastically upon formation of the helicate, points to a very fast energy transfer process, compatible with the electron transfer mechanism, although not proving it.

V. Conclusion

Metal-centered luminescence is fairly well sensitized in the triple stranded homodimetallic helicates $[Ln_2(L^C-2H)_3]$, Ln = Sm (H_2O, D_2O) and Yb (D_2O). The absolute quantum yield of the ligand-centered luminescence decreases dramatically upon formation of the helicates because of a large enhancement in the intersystem crossing rate constant and subsequent energy transfer onto the metal ions results in the observation of metal-centered luminescence. Both the quantum yields and lifetimes of the metal-centered luminescence of the helicates in D_2O are large compared to other values reported in the literature, pointing to these systems as potential luminescent probes for applications in bioanalyses. Indeed, ligand L^C can be easily derivatized in the 4-position of the pyridines[50] so that grafting of adequate sensitizing groups is within reach.

Pioneer work for the calculation of energy transfer rates and emission quantum yield in the Sm^{III} helicate leads to a good agreement between experimental and theoretical quantum yield of the metal centered emission, indicating that the theoretical approach used is adequate. We have shown that the main energy stream from the ligand to the metal ion goes through the triplet state through an exchange mechanism. This type of theoretical modeling of energy transfer processes opens the way for a more rational design of samarium luminescent probes.

Acknowledgment. We gratefully acknowledge Professor Jörma Hölsä (University of Turku) for providing the wave functions of Sm^{III} in SmOCl and Mr M. Hollenstein (University of Bern) for the synthesis of the ligand. F.R.G.S. is indebted to CNPq (Brazilian agency) for a stipend. This work is supported through grants from the Swiss National Science Foundation.

References and Notes

(1) Bünzli, J.-C. G. In *Lanthanide Probes in Life, Chemical and Earth Sciences. Theory and Practice*; Bünzli, J.-C. G., Choppin, G. R., Eds.; Elsevier Science: Amsterdam, 1989.
(2) Parker, D. *Coord. Chem. Rev.* **2000**, *205*, 109.
(3) Yam, V. W. W.; Lo, K. K. W. *Coord. Chem. Rev.* **1999**, *184*, 157.
(4) Hemmilä, I.; Ståhlberg, T.; Mottram, P. *Bioanalytical Applications of Labeling Technologies*: Wallac Oy: Turku, Finland, 1995.
(5) Mathis, G. In *Rare Earths*; Saez Puche, R., Caro, P., Eds.; Editorial Complutense: Madrid, 1998.
(6) Capecchi, S.; Renault, O.; Moon, D.-G.; Halim, M.; Etchells, M.; Dobson, P. J.; Salata, O. V.; Christou, V. *Adv. Mater.* **2000**, *12*, 1591.
(7) Hemmilä, I. *J. Alloys Compnds.* **1995**, *225*, 480.
(8) Maupin, C. L.; Parker, D.; Williams, J. A. G.; Riehl, J. P. *J. Am. Chem. Soc.* **1998**, *120*, 10563.
(9) Faulkner, S.; Beeby, A.; Carrié, M.-C.; Dadabhoy, A.; Kenwright, A. M.; Sammes, P. G. *Inorg. Chem. Commun.* **2001**, *4*, 187.
(10) Wolbers, M. P. O.; Van Veggel, F. C. J. M.; Peters, F. G. A.; Van Beelen, E. S. E.; Hofstraat, J. W.; Geurts, F. J.; Reinhoudt, D. N. *Chem. Eur. J.* **1998**, *4*, 772.
(11) Elhabiri, M.; Scopelliti, R.; Bünzli, J.-C. G.; Piguet, C. *J. Am. Chem. Soc.* **1999**, *121*, 10747.
(12) Bünzli, J.-C. G.; Piguet, C. In *Encyclopedia of Materials: Science and Technology*; Pergamon: New York, 2001; Vol. 5, p 446ff.
(13) de Sá, G. F.; Malta, O. L.; Donega, C. D.; Simas, A. M.; Longo, R. L.; Santa-Cruz, P. A.; da Silva, E. F. *Coord. Chem. Rev.* **2000**, *196*, 165.
(14) Gonçalves e Silva, F. R.; Longo, R. L.; Malta, O. L.; Piguet, C.; Bünzli, J.-C. G. *Phys. Chem. Chem. Phys* **2000**, *2*, 5400.
(15) Bünzli, J.-C. G.; Mabillard, C. *Inorg. Chem.* **1986**, *25*, 2750.
(16) Wolsey, W. C. *J. Chem. Educ.* **1973**, *50*, A335.
(17) Glasoe, P. K.; Long, F. A. *J. Phys. Chem.* **1960**, *64*, 188.
(18) Skoog, D. A.; West, D. M. *Principles of Instrumental Analysis*; Holt, Rinehart and Winston: New York, 1971.
(19) Meech, S. R.; Phillips, D. C. *J. Photochem.* **1983**, *23*, 193.
(20) Magde, D.; Brannon, J. H.; Cremers, T. L.; Olmsted, J., III. *J. Phys. Chem.* **1979**, *83*, 696.
(21) Houten, J. V.; Watts, R. J. *J. Am. Chem. Soc.* **1976**, *98*, 4853.
(22) Charles, R. G.; Ohlmann, R. C. *J. Inorg. Nucl. Chem.* **1965**, *27*, 255.

(23) Meshkova, S. B.; Topilova, Z. M.; Bolshoy, D. V.; Beltyukova, S. V.; Tsvirko, M. P.; Venchikov, V. Y. *Acta Phys. Polonica A* **1999**, *95*, 983.

(24) Malta, O. L. *J. Lumin.* **1997**, *71*, 229.

(25) Malta, O. L.; Gonçalves e Silva, F. R. *Spectrochim. Acta A* **1998**, *54*, 1593.

(26) Carnall, W. T., Crosswhite, H, and Crosswhite, H. M. *Energy Level Structure and Transition Probabilities of the Trivalent Lanthanides in LaF_3*; Argonne National Laboratory: Argonne, IL, 1997.

(27) Malta, O. L.; Gonçalves e Silva, F. R.; Longo, R. L. *Chem. Phys. Lett.* **1999**, *307*, 518.

(28) Gonçalves e Silva, F. R.; Malta, O. L. *J. Alloys Compnds.* **1997**, *250*, 427.

(29) Malta, O. L.; Brito, H. F.; Menezes, J. F. S.; Gonçalves e Silva, F. R.; Alves Jr., S.; Farias, F. S., Jr.; De Andrade, A. V. M. *J. Lumin.* **1997**, *75*, 255.

(30) De Andrade, A. V. M.; Longo, R. L.; Simas, A. M.; de Sá, G. F. *J. Chem. Soc., Faraday Trans.* **1996**, *92*, 1835.

(31) Carnall, W. T.; Fields, P. R.; Rajnak, K. *J. Chem. Phys.* **1968**, *49*, 4424.

(32) Rodriguez-Ubis, J.-C.; Sedano, R.; Barroso, G.; Juanes, O.; Brunet, E. *Helv. Chim. Acta* **1997**, *80*, 86.

(33) Kimura, T.; Kato, Y. *J. Alloys Compnds.* **1995**, *225*, 284.

(34) Xu, Y. Y.; Hemmilä, I.; Lövgren, T. *Analyst* **1992**, *117*, 1061.

(35) Morin, M.; Bador, R.; Dechaud, H. *Anal. Chim. Acta* **1989**, *219*, 67.

(36) Rigault, S.; Piguet, C.; Bünzli, J.-C. G. *J. Chem. Soc., Dalton Trans.* **2000**, 2045.

(37) Gamelin, D. R.; Luthi, S. R.; Güdel, H. U. *J. Phys. Chem. B* **2000**, *104*, 11045.

(38) Klink, S. I.; Grave, L.; Reinhoudt, D. N.; Van Veggel, F. C. J. M.; Werts, M. H. V.; Geurts, F. A. J.; Hofstraat, J. W. *J. Phys. Chem. A* **2000**, *104*, 5457.

(39) Dickins, R. S.; Howard, J. A. K.; Maupin, C. L.; Moloney, J. M.; Parker, D.; Riehl, J. P.; Siligardi, G.; Williams, J. A. G. *Chem. Eur. J.* **1999**, *5*, 1095.

(40) Werts, M. H. V.; Verhoeven, J. W.; Hofstraat, J. W. *J. Chem. Soc., Perkin Trans. 2* **2000**, 433.

(41) Klink, S. I.; Hebbink, G. A.; Grave, L.; Van Veggel, F. C. J. M.; Reinhoudt, D. N.; Slooff, L. H.; Polman, A.; Hofstraat, J. W. *J. Appl. Phys.* **1999**, *86*, 1181.

(42) Wolbers, M. O.; Van Veggel, F. C. J. M.; Snellink-Rüel, B. H. M.; Hofstraat, J. W.; Geurts, F. A. J.; Reinhoudt, D. N. *J. Chem. Soc., Perkin Trans. 2* **1998**, 2141.

(43) Buono-Core, G. E.; Li, H.; Marciniak, B. *Coord. Chem. Rev.* **1990**, *99*, 55.

(44) Malta, O. L.; Brito, H. F.; Menezes, J. F. S.; Gonçalves e Silva, F. R.; Donega, C. D.; Alves, S. *Chem. Phys. Lett.* **1998**, *282*, 233.

(45) Petoud, S.; Bünzli, J.-C. G.; Glanzman, T.; Piguet, C.; Xiang, Q.; Thummel, R. P. *J. Lumin.* **1999**, *82*, 69.

(46) Guldi, D. M.; Mody, T. D.; Gerasimchuk, N. N.; Magda, D.; Sessler, J. L. *J. Am. Chem. Soc.* **2000**, *122*, 8289.

(47) Murov, S. L.; Carmichael, I.; Hug, G. L. *Handbook of Photochemistry*; M. Dekker Inc.: New York, 1993.

(48) Abusaleh, A.; Meares, C. F. *Photochem. Photobiol.* 1984, *39*, 763.

(49) Horrocks, W.deW. Jr.; Bolender, J. P.; Smith, W. D.; Supkowski, R. M. *J. Am. Chem. Soc.* **1997**, *119*, 5972.

(50) Platas, C.; Elhabiri, M.; Hollenstein, M.; Bünzli, J.-C. G.; Piguet, C. *J. Chem. Soc., Dalton Trans.* **2000**, 2031.